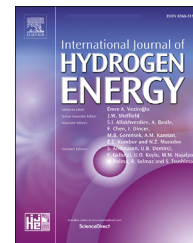




ELSEVIER

Available online at www.sciencedirect.com

ScienceDirect

journal homepage: www.elsevier.com/locate/he

Comparison of theoretical methods of the hydrogen storage capacities of nanoporous carbons

I. Cabria

Departamento de Física Teórica, Atómica y Óptica, Universidad de Valladolid, 47011 Valladolid, Spain

HIGHLIGHTS

- Comparison of hydrogen storage capacities obtained using five theoretical methods.
- Prediction of storage capacities of graphene slit-shaped pores.
- New theoretical method to calculate capacities that includes molecular interactions.

ARTICLE INFO

Article history:

Received 31 January 2020

Received in revised form

14 April 2020

Accepted 24 April 2020

Available online xxx

Keywords:

Hydrogen storage

Hydrogen physisorption

Nanoporous carbons

ABSTRACT

The hydrogen storage capacities of nanoporous carbons, simulated as graphene slit-shaped pores, have been calculated using simple theoretical methods that do not involve computationally expensive calculations. The theoretical methods calculate the storage of hydrogen molecules on a solid porous material by using the Equation Of State, EOS, of the hydrogen gas and the interaction potential energy of H₂ with the surfaces of the pores of the material. Calculations have been carried out using the same interaction potential energy and empirical EOS. The interaction potential energy is obtained from calculations of H₂ on graphene, using a DFT-based method that includes the dispersion interactions. The storage capacities have been calculated as a function of pressure in the range 0.1–25 MPa, of pore width in the range 4.7–20 Å and at 80.15 and 298.15 K. The storage capacities obtained with the methods are compared and the advantages and limitations of the methods are discussed, as well as the storage capacities predicted by the methods for wide pores. These simple theoretical methods are useful to design novel materials for hydrogen storage.

© 2020 Hydrogen Energy Publications LLC. Published by Elsevier Ltd. All rights reserved.

Introduction

Hydrogen cars are an alternative to the present fossil fuel based vehicles. The storage of hydrogen on-board of the vehicle is one of the main technological problems to deploy the hydrogen vehicles in a large scale basis. The U.S. Department Of Energy, DOE, established the on-board hydrogen storage targets for 2020 as 4.5 wt% and 0.030 kg H₂/L at room

temperature and moderate pressures [1]. Among the methods to storage hydrogen on-board, the storage on nanoporous solid materials has been intensely investigated [2–5]. Physisorption is the main mechanism of storage on solid nanoporous materials, such as nanoporous carbons [6–14], porous polymers [15–17] and Metal-Organic Frameworks (MOFs) [18–21].

Theoretical methods are very useful tools to understand the role of physisorption on the storage capacities of solid

E-mail address: ivan.cabria@uva.es.<https://doi.org/10.1016/j.ijhydene.2020.04.212>

0360-3199/© 2020 Hydrogen Energy Publications LLC. Published by Elsevier Ltd. All rights reserved.

nanoporous materials and to design solid nanoporous materials with high storage capacities for on-board hydrogen storage. Grand Canonical Monte Carlo (GCMC) and Molecular Dynamics (MD) simulations are computationally very expensive. There are simple theoretical methods of the hydrogen storage on nanoporous solid materials that are not computationally expensive and that take into account the main features of the equilibrium between the adsorbed and compressed phases inside porous materials [22–27]. The equations of those simple methods are based on physical hypothesis and allow us more insight into the physics of the storage of hydrogen than the equations of the GCMC and MD simulations.

The simple theoretical methods predict different storage capacities. Which method is the most accurate is an open question. The methods are approaches to the real world. A comparison with experimental results of a given porous material could decide which is the most accurate method. To perform that comparison a perfect or at least reasonably accurate knowledge of the geometry and size of the pores of the porous material would be necessary. However, this type of information is not provided by the experiments. In the case of nanoporous carbons, the pore size distribution (PSD) is reported by some experimental papers. The PSD depends on the type of gas used to obtain it and is not a direct measure.

Since it is not possible to be certain about which is the most accurate method, the best we can do is to select a pore model and to calculate the storage capacities of the pore according to the different simple methods. The predicted storage capacities, for a given pressure, temperature and pore width, will be the interval of values reported by the theoretical methods, instead of a single numerical value.

Among the solid nanoporous materials, nanoporous carbons are a wide family or group of materials. Experiments [28] indicate that nanoporous carbons are made mainly of slit-shaped pores: Two graphene parallel layers separated a distance of a few nanometers. This graphene slit-shaped pore geometry is the model studied in this paper.

The goal of this paper is to calculate and compare the hydrogen storage capacities obtained with three published theoretical methods, the Langmuir (LM) [22,23], the Peng-Morris (PM) [24] and the Quantum-Thermodynamic (QT) method [25–27], plus two new proposed methods: The Self-Consistent Peng-Morris (SCPM) method, a modification of the original PM method, and the QT1, a slight modification of the original QT method. Another goal is to predict the storage capacities for wide pores within the interval given by the combined results of the theoretical methods.

Calculations and analysis of the gravimetric and volumetric capacities of nanoporous carbons simulated as graphene slit-shaped pores (See Fig. 1) have been carried out, using five different theoretical methods of the hydrogen storage on nanoporous solid materials. The common features and the differences between the capacities obtained with the five methods are analyzed and discussed. This paper is organized as follows. Section [Pore model](#) is a brief description of the theoretical methods. The storage capacities obtained with the five methods as a function of the pore width, pressure and temperature are compared and discussed in Section [Theoretical methods of hydrogen storage on porous materials](#),

together with the capacities predicted by the methods for wide pores.

Pore model

The pore model (shape, geometry and composition), the interaction potential energy $V(z)$ of H_2 on a single graphene sheet, where z is the H_2 -graphene distance, and the equation of state of hydrogen will be the same on the five methods. The pore model will be the graphene slit-shaped pore (See Fig. 1).

The interaction potential energy $V(z)$ was obtained from RVV10 calculations of H_2 on a single graphene sheet. This potential was published and analyzed previously [29]. The EOS of hydrogen used in the five methods to calculate the molar volume, v_{mol} , and/or the chemical potential, μ , is the Mills-Younglove EOS [26] for pressures up to 1500 MPa and the Vinet EOS [30] for pressures higher than 1500 MPa. The Mills-Younglove is valid up to 1500 MPa. The parameters selected for the Vinet EOS are valid between 50 and 26,500 MPa [31,32].

Fig. 2 illustrates the graphene slit pore potential, $V_{slit\ pore}(z) = V(z) + V(w - z)$, for five pore widths w : 6, 7, 8, 10 and 12 Å. $V(z)$ is the interaction potential energy curve between a H_2 molecule and a single graphene sheet, z is the H_2 -sheet surface distance and w is the distance between the two sheets of the slit-shaped pore and is also the pore width (See Fig. 1). In a slit pore there are two flat parallel graphene sheets, and therefore the slit pore potential, is the sum of the potentials of the two graphene sheets, separated a distance w , $V(z) + V(w - z)$ (See Fig. 2).

The slit pore potential in Fig. 2 shows a single deep minimum for narrow slit pores (6 and 7 Å), and two separated minima for larger pore widths (8, 10 and 12 Å), which correspond to each of the graphene sheets.

Theoretical methods of hydrogen storage on porous materials

The theoretical methods studied calculate the gravimetric and volumetric capacities of the adsorbed hydrogen phase at a given pressure of the compressed phase, P_{com} and temperature T . The methods calculate the molar volume of the adsorbed hydrogen phase, v_{mol} , which depends on P_{com} and T , and the number of moles of the adsorbed phase.

The QT and QT1 methods calculate first the molar volume and then, the number of moles of the adsorbed phase, n_{ads} , as $V_{adsorbed}/v_{mol}$, where $V_{adsorbed}$ is the volume of the adsorbed hydrogen phase. The PM, SCPM and LM methods calculate first the number of moles and then, the molar volume of the adsorbed phase as $v_{mol} = V_{adsorbed}/n_{ads}$. These two magnitudes are used to calculate the volumetric and gravimetric storage capacities of the hydrogen adsorbed phase.

The volumetric capacity in kg/L is calculated as:

$$v_c = \frac{a}{v_{mol}} \frac{V_{adsorbed}}{V_{pore}}, \quad (1)$$

where a is a conversion factor, to convert from moles to kg of hydrogen, and $V_{adsorbed}$ and V_{pore} are the volumes of the adsorbed hydrogen phase and of the pore, respectively.

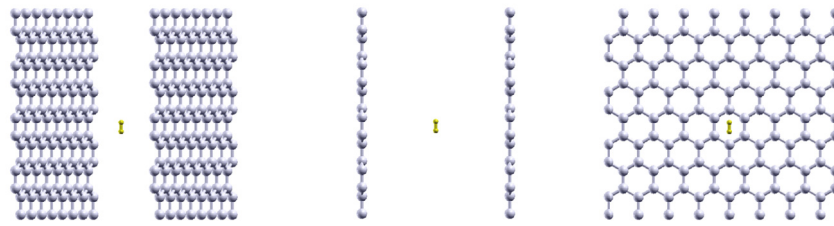


Fig. 1 – Three views of a graphene slit-shaped pore with one hydrogen molecule inside. The two graphene sheets are flat and parallel.

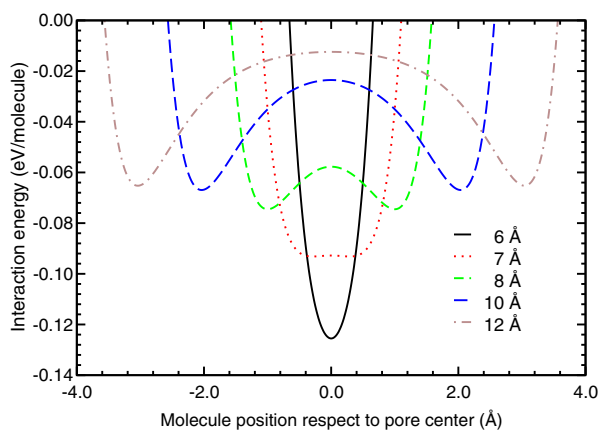


Fig. 2 – Interaction potential energy of a slit-shaped graphene pore, obtained in RVV10 calculations, for several pore widths: 6, 7, 8, 10 and 12 Å.

The gravimetric storage capacity of the adsorbed phase is obtained as follows. First, the number of moles is used to calculate the mass of hydrogen inside the graphene slit-shaped pore as:

$$M_{H\ ads} = n_{ads} N_A 2m_{H\ atom}, \quad (2)$$

where N_A is the Avogadro number and $m_{H\ atom}$ is the mass of a hydrogen atom. Finally, the gravimetric hydrogen storage capacity of the adsorbed phase in weight per cent, wt%, is defined as:

$$g_c = 100 \frac{M_{H\ ads}}{M_{H\ ads} + M_{adsorbent\ material}}, \quad (3)$$

where $M_{adsorbent\ material}$ is the mass of the adsorbent material. In the case of graphene slit pores, $M_{adsorbent\ material}$ is the mass of the two graphene sheets.

As regards to the pressure of the adsorbed phase, P_{ads} , which depends on P_{com} and T , the QT and QT1 methods calculate the pressure of the adsorbed phase and use this pressure to calculate the molar volume of the adsorbed phase as $v_{mol} = v_{mol}(P_{ads}, T)$. Then, these methods calculate the number of moles. The PM and SCPM methods calculate the local pressures of the adsorbed phase, and then, use them to calculate the local molar volumes, the number of moles and the molar volume, in this order. The LM method does not

calculate any pressure of the adsorbed phase and calculates first and directly the number of moles and then, the molar volume.

These are the definitions and units of the capacities presented in this paper. The methods and this paper deal with and analyze the storage capacities of the adsorbed phase of H_2 . In the next subsections we will explain in some detail the calculation of the molar volume and number of moles in the five methods studied. Two of the methods are modifications or variations of another methods. We will explain also a variant of the QT that includes the interaction between the H_2 molecules self-consistently. It is called the Self-Consistent QT method, SCQT.

The Langmuir method

The basic idea of the Langmuir, LM, method is that the molecules are adsorbed on the surface forming a single layer. This method is considered a classical method. Hydrogen storage capacities on porous materials can be calculated using this method. The maximum number of molecules in the adsorbed phase, in this method, is given by $N_{max} = S_{adsorbent}/S_{molecule}$, where $S_{adsorbent}$ is the surface of the adsorbent material and $S_{molecule}$ is the dynamic surface of the hydrogen molecule. In the present case, $S_{adsorbent}$ is the surface of the two walls of the slit pore.

The number of moles of the adsorbed phase of H_2 is n_{ads} and is given by $n_{ads} = N_{max}f/N_A$, where N_A is the Avogadro number and the factor f is given by:

$$f = \frac{1}{1 + e^{\beta(\mu(P,T) - E_{binding})}}, \quad (4)$$

where $\mu(P, T)$ is the chemical potential of hydrogen gas at pressure P and temperature T , $\beta = 1/k_B T$, k_B is the Boltzmann constant and $E_{binding}$ is the potential depth of the interaction potential of the pore. The chemical potential was obtained from the Mills-Younglove EOS [26]. Finally, the molar volume of the adsorbed phase is obtained as $v_{mol} = V_{adsorbed}/n_{ads}$. This is the fastest method.

The Peng-Morris method

The Peng-Morris method and its details can be found in Ref. [24]. In this method, the equilibrium between the two

hydrogen phases inside a slit-shaped pore, compressed and adsorbed, implies that the local pressure of the adsorbed phase at location z , is given by:

$$P_{\text{local adsorbed}}(z, T) = P_{\text{com}} e^{-\beta V_{\text{slit pore}}(z)}. \quad (5)$$

where $V_{\text{slit pore}}(z)$ is the interaction energy potential at location z inside the slit-shaped pore. The molar density at point z is given by:

$$\rho(z) = 1 / v_{\text{mol}}(P_{\text{local adsorbed}}(z, T)), \quad (6)$$

where v_{mol} is the local molar volume given by the Mills-Younglove EOS, as it was pointed out in a former section. Finally, the number of moles of the adsorbed phase is calculated by means of:

$$n_{\text{ads}} = \int_{V_{\text{adsorbed phase}}} \rho(z) dV, \quad (7)$$

where the integration is over the volume of the adsorbed phase. The molar volume of the adsorbed phase is obtained as $v_{\text{mol}} = V_{\text{adsorbed}}/n_{\text{ads}}$.

Peng and Morris pointed out that the PM method yields sometimes nonphysical results, because some local pressures are outside the validity range of the used EOS [24]. The tests of the PM method performed with the Mills-Younglove EOS reported that the local pressure is very high and outside the validity limits of the Mills-Younglove EOS for some values of the pressure of the compressed phase, temperature and interaction potential energy. At certain points z the interaction potential energy can be very negative and the local pressure, $P_{\text{local adsorbed}}(z, T)$, can be too high at low temperatures. Hence, to solve this problem and to avoid nonphysical results, for local pressures $P_{\text{local adsorbed}}(z, T)$ larger than 1500 MPa, the Vinet EOS [30] instead of the Mills-Younglove EOS has been used in the present research. The values of the parameters of the Vinet EOS for hydrogen at low and room temperatures were taken from Refs. [31,32], respectively, and are valid between 50 and 26,500 MPa.

LM and PM methods are classical methods. LM is a one layer method. PM method takes into account the potential energy at different values of z and hence, somehow can be considered a multiple layer method. The PM method is about 300 times slower than the LM method, due to the calculations to obtain n_{ads} , Eq. (7).

The self-consistent Peng-Morris method

The Self-Consistent Peng-Morris method is a modification of the original PM method. The SCPM method includes in a self-consistent manner the interaction between neighbour H_2 molecules. This modification improves a big deal the original PM method at low temperature.

The PM method yields very high local pressures of the adsorbed phase at certain locations z and at low temperatures. The energy inserted in Eq. (5) to obtain the local pressure at z , $P_{\text{local adsorbed}}(z, T)$, is the interaction potential energy of one H_2 molecule with the slit pore, for a H_2 -surface distance z , $V_{\text{slit pore}}(z)$. This energy could be so deep for some points z that the pressure $P_{\text{local adsorbed}}(z, T)$ obtained from Eq. (5) could be very high, especially at low temperatures. We will show in the

discussion of the results the average local pressures obtained with the PM and the SCPM methods.

In the original PM method, only the interaction energy between the slit pore and a H_2 molecule located at a distance z from the slit pore surface is considered. In the proposed method, the SCPM, the interaction energy between the molecule at z and the first neighbour molecules is also considered, $E_{\text{H}_2\text{H}_2}(P_{\text{local adsorbed}}(z, T))$. This energy depends on the local pressure of the adsorbed phase and the temperature T .

The local pressure is calculated as

$$P_{\text{local adsorbed}}(z, T) = P_{\text{com}} e^{-\beta E(z)}. \quad (8)$$

where the energy $E(z)$ is the total energy, i.e., the sum of the interaction potential energy of one H_2 molecule with the slit pore and with the nearest neighbour H_2 molecules at $P_{\text{local adsorbed}}(z, T)$ and T : $V_{\text{slit pore}}(z) + E_{\text{H}_2\text{H}_2}(P_{\text{local adsorbed}}(z, T))$.

The energy $E_{\text{H}_2\text{H}_2}(P_{\text{local adsorbed}}(z, T))$ is obtained as:

$$E_{\text{H}_2\text{H}_2}(P_{\text{local adsorbed}}(z, T)) = V_{\text{SG}}(r), \quad (9)$$

where r is the average H_2 - H_2 distance at location z of the adsorbed phase of hydrogen and V_{SG} is the Silvera-Goldmann interaction potential energy between two H_2 molecules [33].

The average H_2 - H_2 distance r is obtained from the local molar volume at z as:

$$r = \sqrt[3]{v_{\text{mol}}(P_{\text{local adsorbed}}(z, T))/N_A}, \quad (10)$$

where v_{mol} is the local molar volume given by the Mills-Younglove EOS, and N_A is the Avogadro number.

Since the energy $E_{\text{H}_2\text{H}_2}(P_{\text{local adsorbed}}(z, T))$ depends on the local pressure at z , this energy, the local pressure and the local molar volume are related to each other and are calculated self-consistently, starting from the local pressure at z of the original PM method. First, the molar volume at z is calculated using the local pressure, then the average distance r and the energy $E_{\text{H}_2\text{H}_2}(P_{\text{local adsorbed}}(z, T))$ at z are obtained. After these magnitudes are calculated, the total energy $E(z)$ and $P_{\text{local adsorbed}}(z, T)$ are calculated and the cycle is repeated until a self-consistent local pressure is obtained.

The magnitudes $E_{\text{H}_2\text{H}_2}(P_{\text{local adsorbed}}(z, T))$ and $P_{\text{local adsorbed}}(z, T)$ have been calculated self-consistently. The self-consistent cycle stops at the i -th iteration if the absolute change, $\Delta P(i)$, is less than 0.1 MPa or the relative change, $\Delta P(i) / P_{\text{local adsorbed}}(z, T)(i)$, is less than 0.01. The absolute change is given by:

$$\Delta P(i) = |P_{\text{local adsorbed}}(z, T)(i-1) - P_{\text{local adsorbed}}(z, T)(i)|. \quad (11)$$

Once the local pressure and local molar volume are calculated, the rest of the SCPM method is identical to the PM method, i.e., Eqs. (6) and (7) are common to both methods. As regards to the computation time, the SCPM method is about 10 times slower than the PM method.

The quantum-thermodynamic and the QT1 methods

The Quantum-Thermodynamic, QT, method has been described and applied to carbon-based nanopores in previous publications [25–27,34–36]. Hence, the main steps and equations of the methods will be described in a brief manner. The

QT1 method is a slight variation of the QT method and will be discussed at the end of this section.

First, the energies ε_i of the quantum states of the hydrogen molecule in the potential of the slit-shaped pore, $V_{\text{slit pore}}(z)$, are calculated by solving the corresponding Schrödinger equation. Then, the partition function of the adsorbed hydrogen phase, Z_{ads} , at temperature T , is calculated by means of

$$Z_{\text{ads}} = \sum e^{-\beta\varepsilon_i}, \quad (12)$$

where $\beta = 1/k_B T$ and k_B is the Boltzmann constant. The equilibrium constant between the adsorbed and compressed phase, confined in the volume V of the pore, is given by

$$K_{\text{eq}} = Z_{\text{ads}}/Z_{\text{com}}, \quad (13)$$

where Z_{com} is the partition function of the compressed phase. In the case of a slit pore of width w , this partition function is obtained as

$$Z_{\text{com}} = (w - 2w_{\text{excl}}) \sqrt{2\pi m k_B T} / h^2, \quad (14)$$

where m is the mass of one hydrogen molecule and w_{excl} is an exclusion distance due to the steep repulsive part of the interaction potential $V(z)$ near the pore layers. The exclusion distance is equal to the distance at which the repulsive part of the potential $V(z)$ equals one eV.

In the thermodynamic equilibrium, the equilibrium constant K_{eq} is related to the pressures of the compressed and adsorbed phases, P_{com} and P_{ads} , respectively, through the equation:

$$\ln K_{\text{eq}} = \frac{1}{RT} \int_{P_{\text{com}}}^{P_{\text{ads}}} v_{\text{mol}}(P, T) dP. \quad (15)$$

The pressure of the compressed phase, P_{com} , is the pressure P exerted externally to fill the adsorbent material with hydrogen. It is also sometimes called the external pressure.

The molar volume $v_{\text{mol}}(P, T)$ in Eq. (15) is given by the EOS of hydrogen. The EOS used in the method for pressures up to 1500 MPa is the empirical Mills-Younglove EOS explained in. In the QT and QT1 methods the pressures do not reach values higher than 1500 MPa. However, just in case, the method uses the Vinet EOS for pressures higher than 1500 MPa.

Finally, the implicit equation Eq. (15) is solved and the pressure of the adsorbed phase, P_{ads} , for each value of $P_{\text{com}} = P$ and T is obtained. Then, the molar volume of the adsorbed hydrogen phase, $v_{\text{mol}}(P_{\text{ads}}, T)$, is calculated using P_{ads} and the EOS of hydrogen.

As we have explained at the start of this section, the number of moles of the hydrogen adsorbed phase, n_{ads} , is given by,

$$n_{\text{ads}} = V_{\text{adsorbed}} / v_{\text{mol}}(P_{\text{ads}}, T), \quad (16)$$

The QT1 method is similar to the QT method. The only difference is that in the calculation of the partition function Z_{ads} , only the ground state energy ε_i of the molecule is used. Since the QT method uses all the quantum states, it can be considered a multiple layer method, and the QT1 method

can be considered somehow a quantum one layer method. The purpose is to compare a quantum one layer method, QT1, with a classical one layer method, the LM method. As regards to the computation times, the QT and QT1 methods are about 100 times slower than the fastest method, the LM method.

The self-consistent quantum-thermodynamic method

The EOS used in the QT and in all the methods is a real EOS and hence, it includes the effects of the interaction between the H_2 molecules. In the SCPM method that interaction energy, $E_{H_2H_2}(P_{\text{local adsorbed}}(z, T))$, was also included in the interaction potential energy. The QT method (or the standard QT method) does not include the interaction between the molecules in the interaction potential energy. The Self-Consistent QT (SCQT) method includes that interaction in a self-consistent way, similar to the SCPM method. The SCQT method uses the pressure of the adsorbed phase, P_{ads} , instead of the local pressure of the adsorbed phase. As we will show, the difference between the QT and SCQT results is very small.

The potential energy in the SCQT method is given by $V_{\text{slit pore}}(z) + E_{H_2H_2}(P_{\text{ads}})$, like in the SCPM method. The interaction energy between the molecules is given by

$$E_{H_2H_2}(P_{\text{ads}}) = V_{SG}(r_{\text{ads}}), \quad (17)$$

where the H_2 - H_2 distance r_{ads} is given by

$$r_{\text{ads}} = \sqrt[3]{v_{\text{mol}}(P_{\text{ads}})/N_A}. \quad (18)$$

The interaction energy $E_{H_2H_2}(P_{\text{ads}})$ depends on the pressure of the adsorbed phase, which in turn depends on P_{com} and the temperature. The initial value of $E_{H_2H_2}(P_{\text{ads}})$ is calculated using the pressure of the adsorbed phase obtained in the standard QT method and Eq. (17).

After the calculation of $E_{H_2H_2}(P_{\text{local adsorbed}}(z, T))$, the Schrödinger equation of one hydrogen molecule in the potential $V_{\text{slit pore}}(z) + E_{H_2H_2}(P_{\text{local adsorbed}}(z, T))$ is solved, and the energies of the quantum states obtained are used to obtain a new value of P_{ads} . Then, a new value of $E_{H_2H_2}(P_{\text{local adsorbed}}(z, T))$ is obtained and the calculations are repeated.

This self-consistent process stops when the absolute change at the i -th iteration, $\Delta P(i)$, is less than 0.1 MPa or the relative change, $\Delta P(i)/P_{\text{ads}}(i)$, is less than 0.01. The absolute change is given by:

$$\Delta P(i) = |P_{\text{ads}}(i) - P_{\text{ads}}(i-1)|. \quad (19)$$

We have compared the results obtained using the QT and SCQT methods in Figs. 3–5. The results are very similar for low and room temperature, for any pressure and for any pore width. The differences are very small, even at low temperature. The pressure of the adsorbed phase obtained with the QT and SCQT methods is very similar for any value of the pressure of the compressed phase, the temperature and the pore width. This pressure is used to calculate the storage capacities and hence, the capacities are also very similar.

The initial pressure of the adsorbed phase used in the self-consistent process of the SCQT method is not very high and therefore, the changes of the storage capacities due to the self-

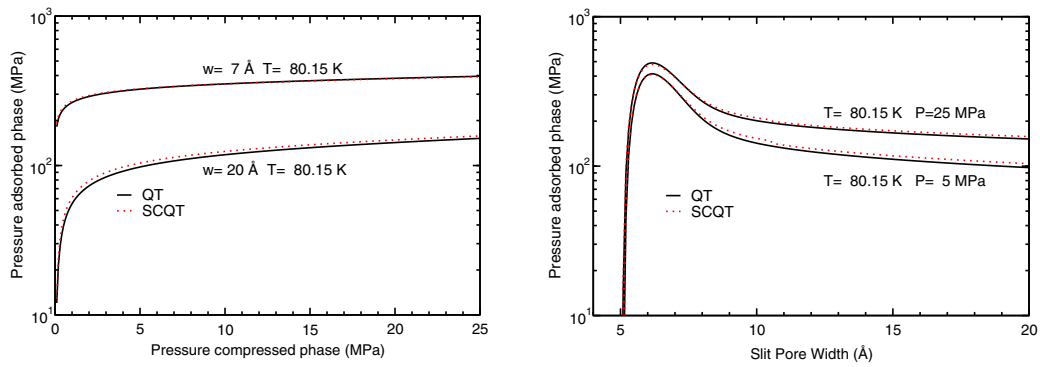


Fig. 3 – Pressure of the adsorbed phase obtained with the QT and SCQT methods at 80.15 K (in logarithmic scale), as a function of the pressure of the compressed phase, for slit-shaped pores of 7 and 20 Å of width, and as a function of the pore width, for 5 and 25 MPa.

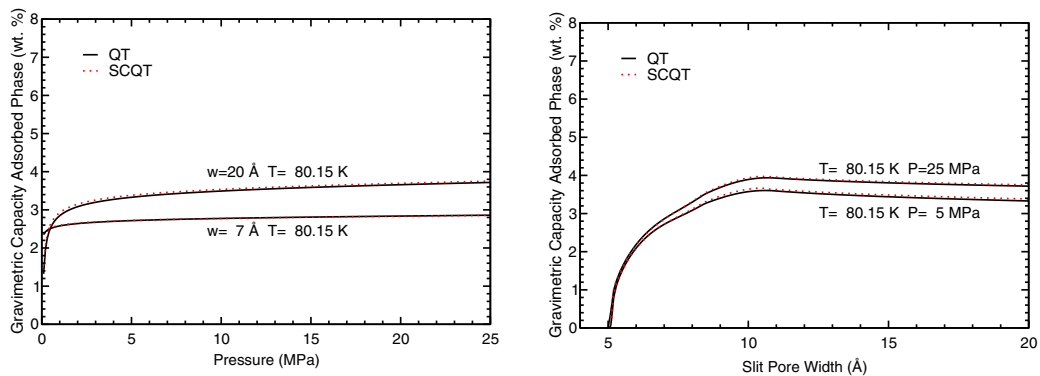


Fig. 4 – Gravimetric storage capacities obtained with the QT and SCQT methods at 80.15 K vs pressure, for pore widths of 7 and 20 Å, and vs pore width at 80.15 K, for 5 and 25 MPa.

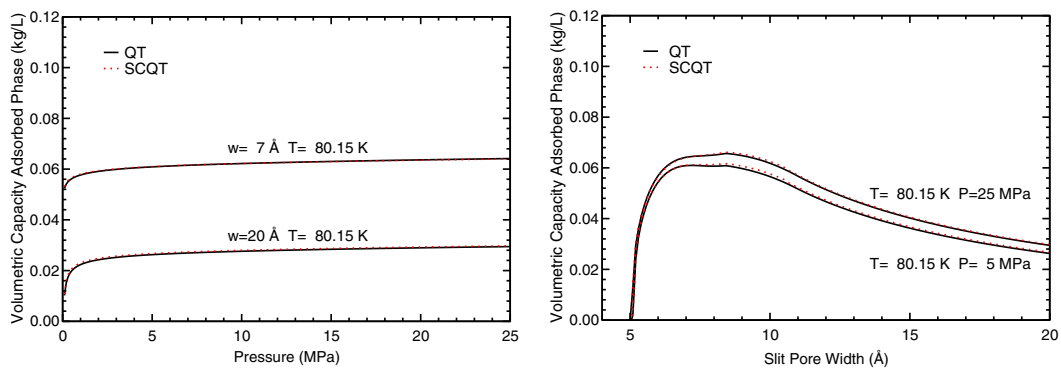


Fig. 5 – Volumetric storage capacities obtained with the QT and SCQT methods at 80.15 K vs pressure, for pore widths of 7 and 20 Å, and vs pore width at 80.15 K, for 5 and 25 MPa.

consistent inclusion of the interaction energy $E_{h_2h_2}(P_{ads})$ are very small.

The main reason to use the QT instead of the SCQT method is the computation time: The QT method is about 1000 times faster than the SCQT method and the results are practically the same. In the QT method, the Schrödinger equation is solved only one time for a fixed pore width. P_{ads} and the storage capacities are calculated for each value of (P_{com}, T) , but using the same energies of the quantum states obtained at the

beginning of the QT method. However, in the SCQT method, the Schrödinger equation has to be solved and P_{ads} has to be calculated self-consistently for each value of (P_{com}, T) , until the convergence is reached. The convergence is reached after 2–5 iterations (2 iterations at room temperature and 5 at low temperature).

An approximate analysis of the computation times of the QT and SCQT methods shows that the QT method is about 1000 times faster. If the number of pairs (P_{com}, T) is N , then the

computation time of the QT method is $t_E + Nt_P$, where t_E is the computation time to solve the Schrödinger equation and t_P is the computation time to obtain P_{ads} and the storage capacities for a pair (P_{com}, T) . In the present research, the calculations of the storage capacities were done for P_{com} between 0.1 and 25 MPa, with a step 0.1 MPa, and for 80.15 and 298.15 K, and hence, N is 500.

The computation time of the SCQT method is $Nn_i(t_E + t_P)$, where n_i is the average number of iterations to reach convergence. Nt_P is about 0.4 times t_E . The computation times of the QT and SCQT methods are given by $t_{QT} = t_E + Nt_P \approx 1.4t_E$ and $t_{SCQT} = Nn_i(t_E + t_P) \approx Nn_it_E$, respectively. The ratio of these two computation times is $t_{SCQT}/t_{QT} \approx Nn_i/1.4$. The average number of iterations n_i is three and N is 500. This implies that the ratio t_{SCQT}/t_{QT} is approximately 1000 and hence, the QT method is about 1000 times faster than the SCQT method.

To close this section, the main properties, the advantages and disadvantages of the methods studied in this work have been briefly summarized in Table 1.

Discussion of results

Pressure of the adsorbed phase at low temperature

The pressure of the adsorbed phase is not the main goal of the theoretical methods, but it is a basic and intermediate step to calculate the volumetric and gravimetric hydrogen storage capacities. The pressure of the adsorbed phase obtained at 80.15 K with the theoretical methods as a function of the pore width, for 5 and 25 MPa, and of the pressure of the compressed phase, for $w = 7$ and 20 Å, is plotted in Figs. 6 and 7, respectively. The pressures of the adsorbed phase of the PM and SCPM methods plotted on those figures are the averages of the local pressures of these methods. The QT and QT1 pressures are not averages. Therefore, the comparison of the pressures of the adsorbed phase is a qualitative comparison. As we explained, the LM method does not calculate a pressure of the adsorbed phase.

The pressure of the adsorbed phase obtained with the theoretical methods follows this order in all the figures, for fixed values of the pore width, pressure and temperature: $P_{ads}(PM) > P_{ads}(SCPM) > P_{ads}(QT) > P_{ads}(QT1)$.

The PM pressures of the adsorbed phase are huge at low temperature for most of the pore widths and pressures

studied (See Figs. 6 and 7). Many PM pressures at low temperature are about five-four orders of magnitude larger than the SCPM, QT and QT1 pressures, and are above 26,500 MPa, the upper limit of validity of the Vinet EOS used in the PM method. The extrapolation of the Vinet EOS beyond 26,500 MPa seems correct [30], but the calculation of the molar volume with the Vinet EOS using pressures higher than 26,500 MPa and of the corresponding storage capacities is not consistent. This means that the PM method is not consistent at low temperature for many pore widths and pressures, even using the Vinet EOS, which is valid at high pressures.

The SCPM pressures at low temperatures are below 26,500 MPa and hence, they are within the validity range of the combined Mills-Younglove and Vinet EOS, and the calculation of the molar volume and the storage capacities is consistent. It can be noticed in Figs. 6 and 7 that the SCPM method corrects the huge and inconsistent values of the pressure of the adsorbed phase obtained with the original PM method at low temperature.

Pressure of the adsorbed phase at room temperature

The pressure of the adsorbed phase obtained at 298.15 K with the theoretical methods as a function of the pore width and of the pressure of the compressed phase is plotted in Figs. 8 and 9. At room temperature, the modification included in the SCPM has a very little impact: The PM and SCPM pressures are of the same order of magnitude and numerically very similar.

At room temperature, the pressure of the adsorbed phase obtained with the theoretical methods follows this order in all the figures, for fixed values of the pore width, pressure and temperature: $P_{ads}(PM)$ and $P_{ads}(SCPM) > P_{ads}(QT) > P_{ads}(QT1)$. The PM pressure of the adsorbed phase is larger than $P_{ads}(SCPM)$ for some values of the pore width and pressure of the compressed phase, not for any value.

Storage capacities at low temperature

The gravimetric and volumetric capacities as a function of the pore width obtained with the five methods at 80.15 K are plotted in Figs. 10 and 11. The dependence of the five capacities on the pore width is, in general, different. Nevertheless, the five capacities have some common features. The capacities have a maximum and then decrease towards a constant value.

Table 1 – Summary of the main properties of the methods.

Property/Method	LM	PM and SCPM	QT, QT1 and SCQT
Use EOS of H ₂	Yes	Yes	Yes
Calculation of v_{mol}	Yes	Yes	Yes
Theory	classical	classical	Quantum
Number of layers	Single	multiple	Multiple
Calculation of P_{ads}	No	yes; local	yes; total
Pressure of the adsorbed phase, P_{ads}	ok	huge and inconsistent at low temperature	Ok
Relative computation time	1	300 and 5000	100, 100 and 10 ⁵

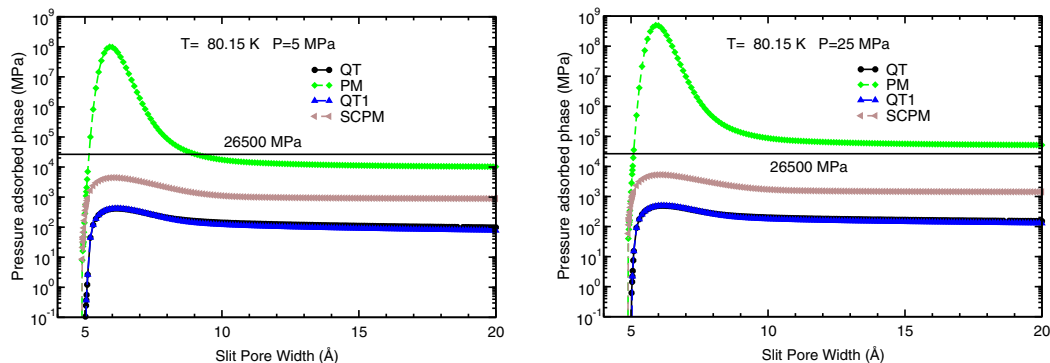


Fig. 6 – Pressure of the adsorbed phase (in logarithmic scale) at 80.15 K as a function of the pore width, for two pressures of the compressed phase: 5 and 25 MPa.

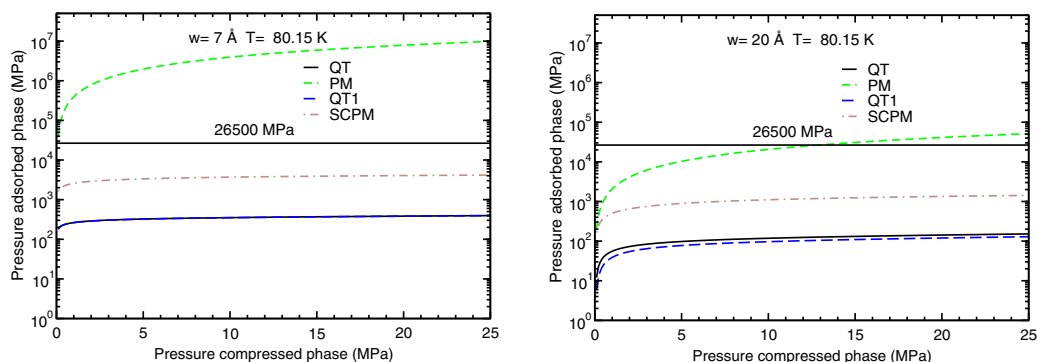


Fig. 7 – Pressure of the adsorbed phase (in logarithmic scale) as a function of the pressure of the compressed phase at 80.15 K and for slit-shaped pores of 7 and 20 Å of width.

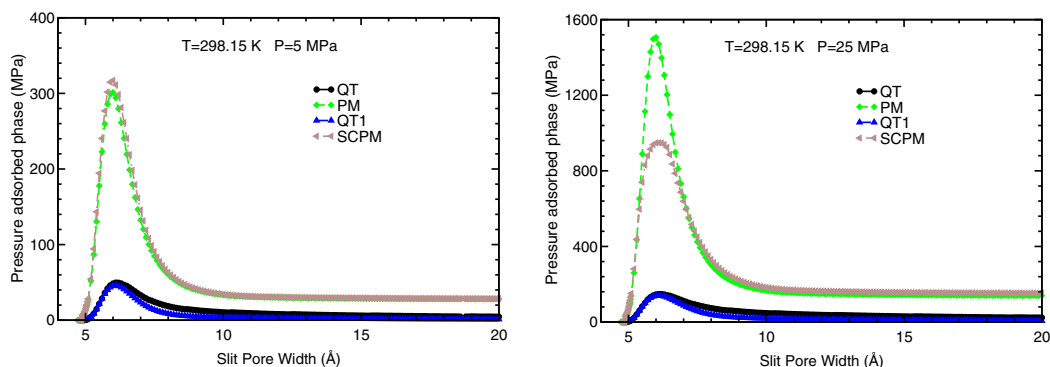


Fig. 8 – Pressure of the adsorbed phase at 298.15 K as a function of the pore width, for two pressures of the compressed phase: 5 and 25 MPa.

At low temperature and above 10 Å, the storage capacities c follow this order: $c_{PM} > c_{SCPM} > \approx c_{LM} > \approx c_{QT} \approx c_{QT1}$, where c stands for g_c and v_c . Below 10 Å there is not a clear hierarchy.

The PM capacities are very different from the capacities obtained with the other methods, including the SCPM method. The SCPM, QT and QT1 capacities have similar numerical values at any pore width, especially at large pore widths.

These results indicate the important influence or impact at low temperatures of the self-consistent inclusion of the interaction between hydrogen molecules into the SCPM method, to improve the original PM method.

QT and QT1 capacities are very similar for any pore width. LM capacities are similar, in some cases very similar, to the SCPM, QT and QT1 capacities for pore widths larger than

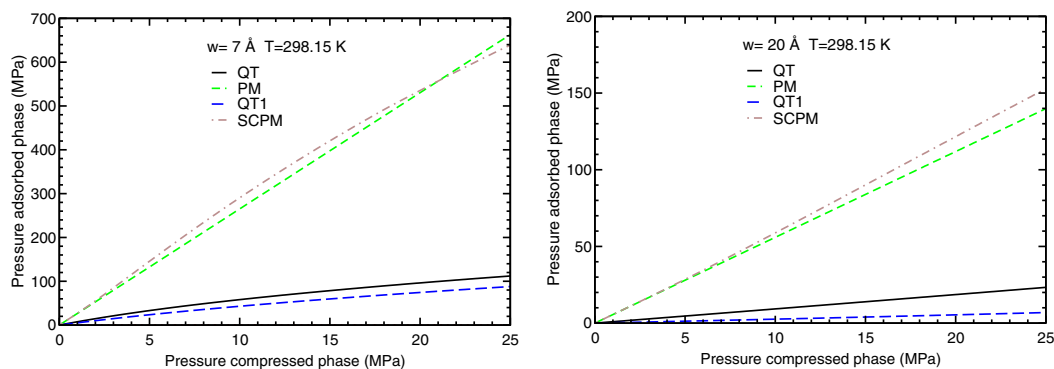


Fig. 9 – Pressure of the adsorbed phase as a function of the pressure of the compressed phase at 298.15 K and for slit-shaped pores of 7 and 20 Å of width.

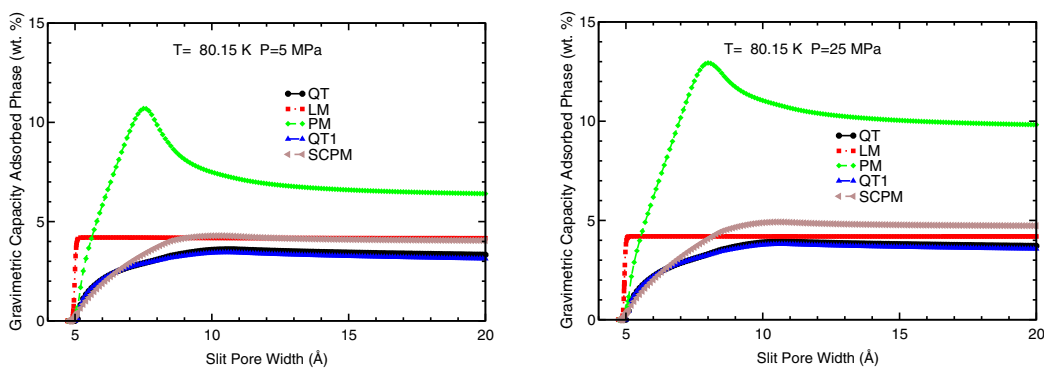


Fig. 10 – Gravimetric storage capacities vs pore width at 80.15 K and for two pressures: 5 and 25 MPa.

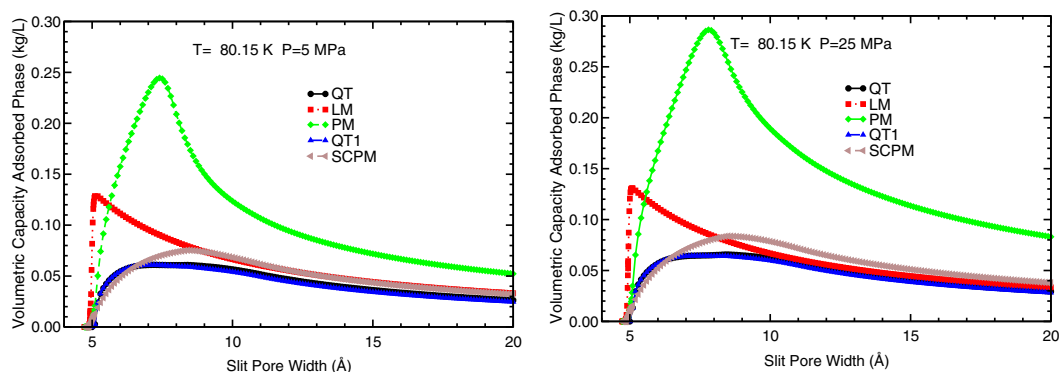


Fig. 11 – Volumetric storage capacities vs pore width at 80.15 K and for two pressures: 5 and 25 MPa.

8–10 Å. The similarity of the LM, SCPM, QT and QT1 capacities for pore widths larger than 8–10 Å indicates that these methods could be somehow, reasonable approaches to the physisorption of H₂ on slit-shaped pores at low temperatures and for large pore widths.

The gravimetric and volumetric capacities as a function of the pressure, the so-called isotherms, at 80.15 K and for pore widths of 7 and 20 Å, are plotted in Figs. 12 and 13. The PM, SCPM, LM, QT and QT1 isotherms have the same dependence on the pressure at low temperature: The isotherms increase

rapidly and tend to a constant or saturation value of the capacity. The constant is different for each method and pore width, 7 and 20 Å. For a pore width of 7 Å, the PM capacity reaches the constant at 5 MPa and the other capacities reach the constant at 1 MPa. For 20 Å, the PM capacities do not reach saturation.

The storage capacities c as a function of the pressure, follow this hierarchy, above 1–2 MPa: $c_{PM} > c_{SCPM} > c_{QT} \approx c_{QT1}$. The LM capacities are below the PM capacities and above the QT and QT1 capacities. The LM capacities are below the SCPM

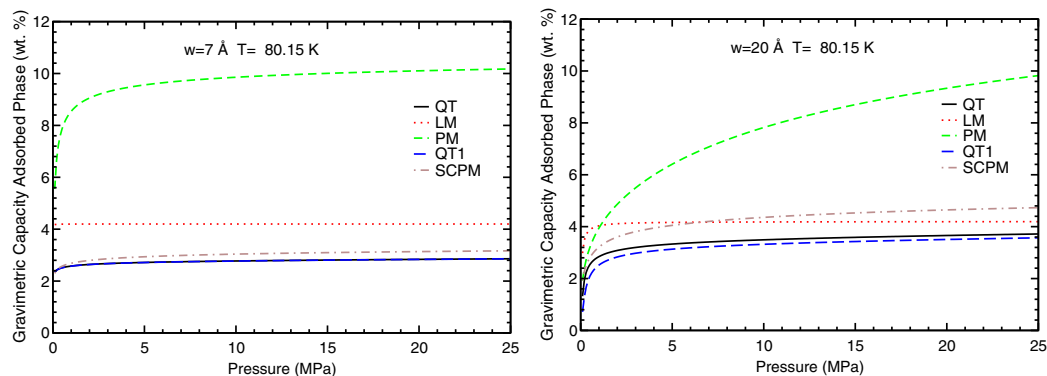


Fig. 12 – Gravimetric storage capacities vs pressure at 80.15 K and for pore widths of 7 and 20 Å.

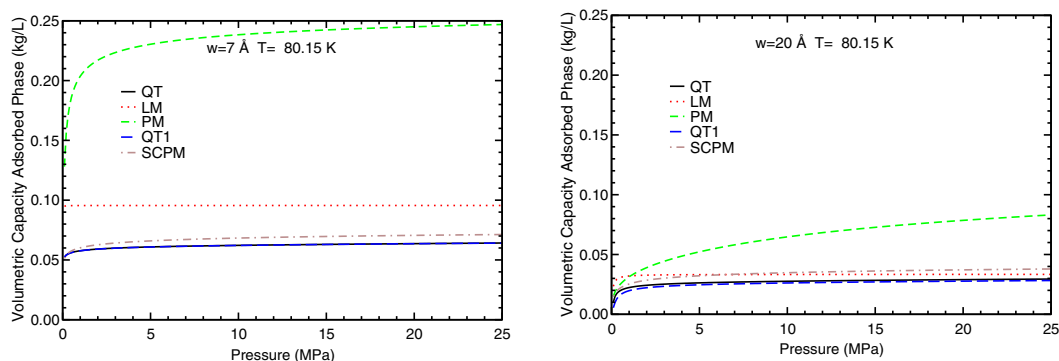


Fig. 13 – Volumetric storage capacities vs pressure at 80.15 K and for pore widths of 7 and 20 Å.

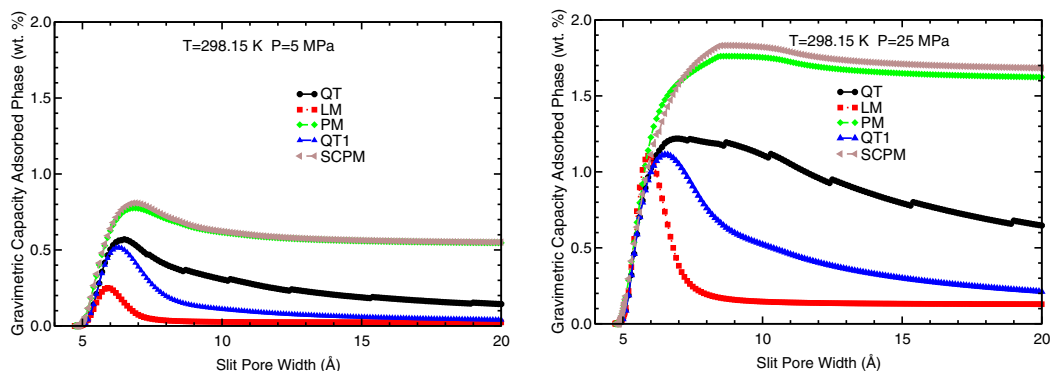


Fig. 14 – Gravimetric storage capacities vs pore width at 298.15 K and for two pressures: 5 and 25 MPa.

capacities for some values of the pore width and pressure, and above them for another values. QT and QT1 capacities are very similar for any value of the pore width and pressure.

The predicted gravimetric storage capacities at 80.15 K, 20 Å and 5 MPa of the LM, QT and SCPM methods are in the interval 3–4 wt %, and at 25 MPa they are in the interval 3.5–5 wt %. As regards to the predicted volumetric capacities at 80.15 K, 20 Å and 25 MPa, the LM, QT and SCPM volumetric

capacities are in the interval 0.025–0.035 kg H₂/L at 5 MPa, and in the interval 0.030–0.040 kg H₂/L at 25 MPa.

Storage capacities at room temperature

The gravimetric and volumetric capacities as a function of the pore width obtained with the five methods at 298.15 K are plotted in Figs. 14 and 15. The dependence or shape of the five

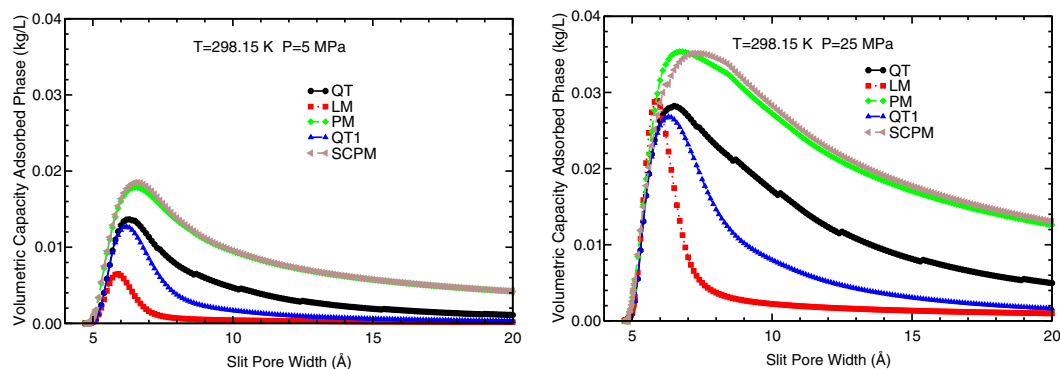


Fig. 15 – Volumetric storage capacities vs pore width at 298.15 K and for two pressures: 5 and 25 MPa.

gravimetric and volumetric capacities on the pore width at 298.15 K is similar: The capacities reach a maximum and then decrease towards a constant value. At room temperature the quantum effects are less pronounced or absent and hence, the dependence of the capacities on the pore width of the five capacities is similar.

The maxima of the capacities vs pore width at room temperature are in the interval 6–7 Å for 5 MPa, and in the interval 6–9 Å for 25 MPa. The exact location of the maximum depends on the method, the pressure and the type of capacity, gravimetric or volumetric. For instance, the gravimetric capacity at 298.15 K and 25 MPa of the LM and PM methods have their maxima at 6 and 9 Å, respectively. Another feature of the maxima is that the one layer methods, LM and QT1, yield capacities with maxima much more abrupt than the multiple layer methods, PM and QT.

The PM and SCPM capacities at room temperature are very similar, almost identical for many pore widths and pressures. The corrections included in the SCPM method have a little impact on the original PM method at room temperature. This was expected, since the local pressure of the adsorbed phase at any z is not so high at room temperature and hence, the energy $E_{h2h2}(P_{local\ adsorbed}(z, T))$ is small compared with $E(z)$, which means that the self-consistent inclusion of $E_{h2h2}(P_{local\ adsorbed}(z, T))$ changes only a little the local pressure and the capacities.

The storage capacities vs pore width obtained with the QT method at room temperature shows some very small discontinuities or jumps at certain values of the pore width (See Figs. 14 and 15). These jumps do not appear in the QT curves at low temperature and do not appear on the QT1 curves at any temperature. The origin of these very small jumps is a quantum effect that occurs for pore widths above 7 Å: As the slit pore width increases the energies of the quantum states increase (are less negative) and K_{eq} , P_{ads} and the storage capacities decrease continuously. At certain values of the pore width, not only the energies change, but also a new quantum state appears, with an energy close to the zero level. This causes a very small increase on K_{eq} , which in turn, causes a very small increase or jump of P_{ads} and the storage capacities. At low temperature, the effect of the new quantum state is so small that K_{eq} and the storage capacities do not suffer jumps and decrease continuously. In the QT1 method, only the

lowest energy is considered. That energy increases continuously as the pore width increases above 7 Å and hence, the QT1 capacities decrease continuously.

At room temperature and above 7 Å, the capacities follow this order: $c(SCPM) > c(PM) > c(QT) > c(QT1) > c(LM)$. QT and QT1 capacities are different at room temperature, while at low temperature are very similar. QT capacities are much larger than QT1 capacities at wide pores and room temperature, because at those pores the relative contribution of the higher eigenvalues is important, compared to the contribution of the ground or lowest eigenvalue. At low temperature, the contribution of the ground state is much more important than the contribution of the other states and hence, the QT and QT1 capacities are very similar.

The gravimetric and volumetric capacities as a function of the pressure at 298.15 K and for pore widths of 7 and 20 Å, are plotted in Figs. 16 and 17. Again, the PM and SCPM capacities at room temperature are very similar. The LM isotherms are linear with the pressure at 298.15 K, the PM and SCPM isotherms are parabolic and the QT and QT1 are parabolic at 7 Å and linear at 20 Å. The parabolic isotherms tend to a linear dependence as the pressure increases.

The LM, QT and SCPM methods predict gravimetric capacities at 298.15 K and 20 Å in the interval 0.01–0.55 wt% at 5 MPa, and in the interval 0.1–1.7 wt% at 25 MPa. Those methods predict volumetric capacities at 298.15 K and 20 Å in the interval 0.001–0.004 kg H₂/L at 5 MPa, and in the interval 0.001–0.013 kg H₂/L at 25 MPa.

Summary and conclusions

We have compared in this paper the hydrogen storage capacities of graphene slit-shaped pores at 80.15 and 298.15 K, for pressures in the range 0.1–25 MPa and pore widths between 4.7 and 20 Å, calculated using five simple theoretical methods. These methods are modelizations of the physisorption of H₂ on porous materials based on different physical ideas. Three methods were published before: The Langmuir (LM), the Peng-Morris (PM) and the Quantum-Thermodynamic (QT) methods. The LM and PM methods are classical methods. The Self-Consistent Peng-Morris, SCPM, method is a new method, and is a modification of the original

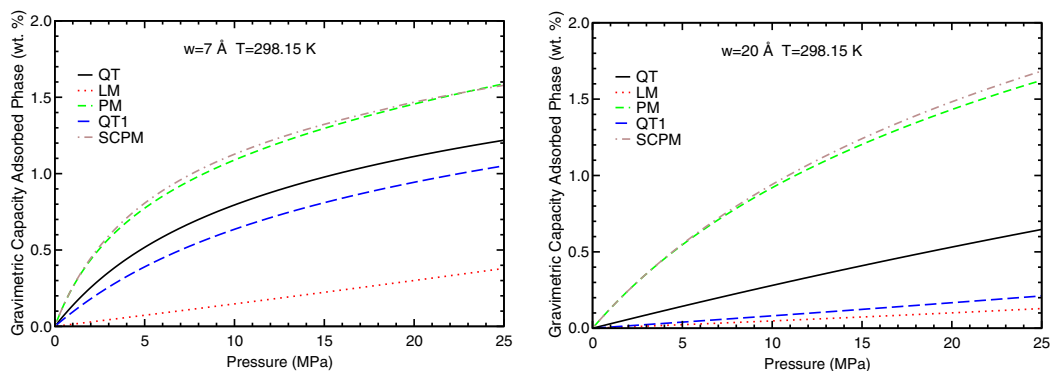


Fig. 16 – Gravimetric storage capacities vs pressure at 298.15 K and for pore widths of $w = 7$ and 20 \AA .

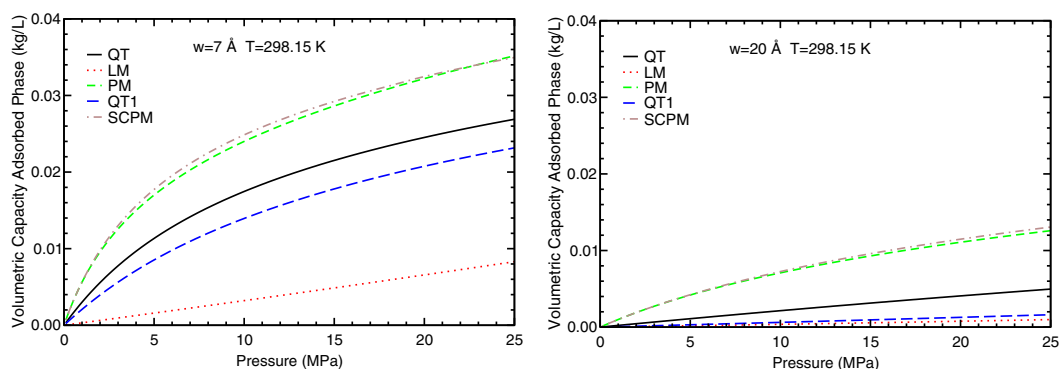


Fig. 17 – Volumetric storage capacities vs pressure at 298.15 K and for pore widths of $w = 7$ and 20 \AA .

PM method. This new method includes the interaction between neighbour H_2 molecules through a self-consistent procedure. The QT1 method is the fifth method and is a slight variation of the QT method. This method considers only the quantum ground state of the H_2 molecule inside a pore.

The PM and SCPM capacities are very different at low temperature. The PM method yields results at low temperature inconsistent with the assumptions of the method, while the SCPM method reports consistent results. At room temperature, however, the PM and SCPM capacities are very similar. The interaction energy between neighbour molecules is large at low temperature and small at room temperature, which means that the self-consistent inclusion of that energy into the SCPM method causes large changes on the capacities at low temperature and small changes at room temperature.

The QT and QT1 capacities are very similar at low temperature. QT capacities are larger than QT1 capacities at room temperature, and much larger at wide pores. At low temperature, the contribution of the quantum ground state of H_2 on the slit-shaped pore is much more important than the contribution of the other states and hence, the QT and QT1 capacities are very similar. At room temperature, the relative contribution of the higher quantum states is important, compared to the ground state contribution, especially in wide pores and this causes larger QT capacities.

The SCPM, QT, QT1 and LM capacities at low temperature and wide pores ($w \geq 8\text{--}10 \text{ \AA}$) are similar. The relative

differences between the capacities obtained with the SCPM, QT, QT1 and LM methods are small at low temperature and larger at room temperature. These facts suggest that these models capture or share more the essence of the physisorption of H_2 on porous materials with large pores at low temperature than at room temperature. At low and room temperature the interaction potential energy of H_2 with the graphene slit-shaped pore is more important at narrow pores than at wide pores. Hence, the differences between the SCPM, QT, QT1 and LM capacities are larger for narrow pores.

According to the results obtained with the SCPM, QT and LM methods, the optimal pore width at room temperature is in the interval $6\text{--}9 \text{ \AA}$. The LM, QT and SCPM methods predict gravimetric capacities at 298.15 K and 20 \AA in the interval $0.01\text{--}0.55 \text{ wt}\%$ at 5 MPa, and in the interval $0.1\text{--}1.7 \text{ wt}\%$ at 25 MPa. Those methods predict volumetric capacities at 298.15 K and 20 \AA in the interval $0.001\text{--}0.004 \text{ kg H}_2/\text{L}$ at 5 MPa, and in the interval $0.001\text{--}0.013 \text{ kg H}_2/\text{L}$ at 25 MPa. The predicted storage capacities are below the DOE targets.

Future research will consist on calculating the storage capacities of porous materials whose structure is known, like MOFs, COFs and others with the five theoretical models and comparing them with the experimental capacities. Another future research path will consist on modelling the nanoporous carbons with more realistic methods: Double, triple layers in the slit-shaped pore, and different pore shapes, like cylindrical, toroidal and spherical.

Acknowledgments

This work was supported under MINECO research project from Spain (Grant PGC2018-093745-B-I00), Junta de Castilla y León (Project No. VA124G18) and the University of Valladolid, Spain. The facilities provided by Centro de Proceso de Datos - Parque Científico of the University of Valladolid are acknowledged.

REFERENCES

- [1] Office of Energy Efficiency & Renewable Energy, Fuel Cell Technologies Office. Materials-based hydrogen storage. 2018. <https://www.energy.gov/eere/fuelcells/materials-based-hydrogen-storage>. [Accessed 26 February 2020].
- [2] Kaneko K, Rodríguez-Reinoso F, editors. Nanoporous materials for gas storage. New York: Springer Singapore; 2019.
- [3] Allendorf MD, Hulvey Z, Gennett T, Ahmed A, Autrey T, Camp J, et al. An assessment of strategies for the development of solid-state adsorbents for vehicular hydrogen storage. *Energy Environ Sci* 2018;11:2784–812.
- [4] Ren J, Musyoka NM, Langmi HW, Mathe M, Liao S. Current research trends and perspectives on materials-based hydrogen storage solutions: a critical review. *Int J Hydrogen Energy* 2017;42:289–311.
- [5] Broom DP, Webb CJ, Hurst KE, Parilla PA, Gennett T, Brown CM, et al. Outlook and challenges for hydrogen storage in nanoporous materials. *Appl Phys A* 2016;122:151.
- [6] Blankenship TS, Balahmar N, Mokaya R. Oxygen-rich microporous carbons with exceptional hydrogen storage capacity. *Nat Commun* 2017;8:1545.
- [7] Blankenship TS, Mokaya R. Cigarette butt-derived carbons have ultra-high surface area and unprecedented hydrogen storage capacity. *Energy Environ Sci* 2017;10:2552–62.
- [8] Mortazavi SZ, Reyhani A, Mirershadi S. Hydrogen storage properties of multi-walled carbon nanotubes and carbon nano-onions grown on single and bi-catalysts including Fe, Mo, Co and Ni supported by MgO. *Int J Hydrogen Energy* 2017;42:24885–96.
- [9] Krasnov PO, Shkaberina GS, Kuzubov AA, Kovaleva EA. Molecular hydrogen sorption capacity of D-schwarzites. *Appl Surf Sci* 2017;416:766–71.
- [10] Sriling P, Wongkoblap A, Tangsathitkulchai C. Computer simulation study for methane and hydrogen adsorption on activated carbon based catalyst. *Adsorption* 2016;22:707–15.
- [11] Sethia G, Sayari A. Activated carbon with optimum pore size distribution for hydrogen storage. *Carbon* 2016;99:289–94.
- [12] Wróbel-Iwaniec I, Díez N, Gryglewicz G. Chitosan-based highly activated carbons for hydrogen storage. *Int J Hydrogen Energy* 2015;40:5788–96.
- [13] Bartolomei M, Carmona-Novillo E, Giorgi G. First principles investigation of hydrogen physical adsorption on graphynes' layers. *Carbon* 2015;95:1076–81.
- [14] Zhang C, Li J, Shi C, He C, Liu E, Zhao N. Effect of Ni, Fe and Fe-Ni alloy catalysts on the synthesis of metal contained carbon nano-onions and studies of their electrochemical hydrogen storage properties. *J Energy Chem* 2014;23:324–30.
- [15] Tian M, Rochat S, Polak-Kraśna K, Holyfield LT, Burrows AD, Bowen CR, et al. Nanoporous polymer-based composites for enhanced hydrogen storage. *Adsorption* 2019;25:889–901. <https://doi.org/10.1007/s10450-019-00065>.
- [16] Lu W. Strategies for hydrogen storage in porous organic polymers. In: Nanostructured materials for next-generation energy storage and conversion hydrogen production, storage, and utilization. Springer; 2017. p. 203–23. chap. 7.
- [17] Liu GL, Wang YX, Shen CJ, Ju ZF, Yuan DQ. A facile synthesis of microporous organic polymers for efficient gas storage and separation. *J Mater Chem* 2015;3:3015–58.
- [18] Zou L, Zhou HC. Hydrogen storage in metal-organic frameworks. In: Nanostructured materials for next-generation energy storage and conversion - hydrogen production, storage, and utilization. Berlin, Heidelberg: Springer-Verlag; 2017. p. 143–70. chap. 5.
- [19] Xia L, Liu Q. Adsorption of H₂ on aluminum-based metal-organic frameworks: a computational study. *Comput Mater Sci* 2017;126:176–81.
- [20] Gygi D, Bloch ED, Mason JA, Hudson MR, González MI, Siegelman RL, et al. Hydrogen storage in the expanded pore metal-organic frameworks M₂(dobpdc) (M = Mg, Mn, Fe, Co, Ni, Zn). *Chem Mater* 2016;28:1128–38.
- [21] Zhu G, Sun Q. Recent advances in computational studies of organometallic sheets: magnetism, adsorption and catalysis. *Comput Mater Sci* 2016;112:492–502.
- [22] Mpourmpakis G, Froudakis GE. Assessing the density functional theory in the hydrogen storage problem. *J Nanosci Nanotechnol* 2008;8:3091–6.
- [23] Ye Y, Ahn CC, Witham C, Fultz B, Liu J, Rinzler AG, et al. Hydrogen adsorption and cohesive energy of single-walled carbon nanotubes. *Appl Phys Lett* 1999;74:2307–9.
- [24] Peng L, Morris JR. Prediction of hydrogen adsorption properties in expanded graphite model and in nanoporous carbon. *J Phys Chem C* 2010;114:15522–9.
- [25] Cabria I. Simulations of volumetric hydrogen storage capacities of nanoporous carbons: effect of dispersion interactions as a function of pressure, temperature and pore width. *Int J Hydrogen Energy* 2020;45:5697–709. <https://doi.org/10.1016/j.ijhydene.2019.03.071>.
- [26] Cabria, López and Alonso|cla07 Cabria I, López MJ, Alonso JA. The optimum average nanopore size for hydrogen storage in carbon nanoporous materials. *Carbon* 2007;45:2649–58.
- [27] Patchkovskii S, Tse JS, Yurchenko SN, Zhechkov L, Heine T, Seifert G. Graphene nanostructures as tunable storage media for molecular hydrogen. *Proc Natl Acad Sci USA* 2005;102:10439–44.
- [28] Park MS, Lee SE, Kim MI, Lee YS. CO₂ adsorption characteristics of slit-pore shaped activated carbon prepared from cokes with high crystallinity. *Carbon Lett* 2015;16:45–50.
- [29] Cabria I, López MJ, Alonso JA. Searching for DFT-based methods that include dispersion interactions to calculate the physisorption of H₂ on benzene and graphene. *J Chem Phys* 2017;146:214104.
- [30] Vinet P, Smith JR, Ferrante J, Rose JH. Temperature effects on the universal equation of state of solids. *Phys Rev B* 1987;35:1945–53. <https://doi.org/10.1103/physrevb.35.1945>.
- [31] Akahama Y, Mizuki Y, Nakano S, Hirao N, Ohishi Y. Raman scattering and X-ray diffraction studies on phase III of solid hydrogen. *IOP Conf Series: J Phys: Conf Series* 2017;950:042060. <https://doi.org/10.1088/1742-6596/950/4/042060>.
- [32] Hemley RJ, Mao HK, Finger LW, Jephcoat AP, Hazen RM, Zha CS. Equation of state of solid hydrogen and deuterium from single-crystal x-ray diffraction to 26.5 GPa. *Phys Rev B* 1990;42:6458–70.

- [33] Silvera IF, Goldman VV. The isotropic intermolecular potential for H₂ and D₂ in the solid and gas phases. *J Chem Phys* 1978;69:4209–13.
- [34] Cabria I, López MJ, Alonso JA. Simulation of the hydrogen storage in nanoporous carbons with different pore shapes. *Int J Hydrogen Energy* 2011;36:10748–59.
- [35] Cabria I, López MJ, Alonso JA. Hydrogen storage capacities of nanoporous carbon calculated by density functional and Møller-Plesset methods. *Phys Rev B* 2008a;78:075415.
- [36] Cabria I, López MJ, Alonso JA. Hydrogen storage in pure and Li-doped carbon nanopores: combined effects of concavity and doping. *J Chem Phys* 2008b;128:144704.